A Multiscale Approach to Synthetic Aperture Radar in Dispersive Random Media

Josselin Garnier[1] **and Knut Sølna**[2]

[1] Laboratoire de Probabilités et Modèles Aléatoires & Laboratoire Jacques-Louis Lions, Université Paris VII, Site Chevaleret, 75205 Paris Cedex 13, France
[2] Department of Mathematics, University of California, Irvine CA 92697

E-mail: garnier@math.univ-paris-diderot.fr, ksolna@math.uci.edu

Abstract. We consider Synthetic Aperture Radar (SAR) image formation in the situation when the propagation medium is random and dispersive. The propagation model is the Klein-Gordon equation with a random index of refraction and a random dispersive term. We show via a multiscale analysis how the medium heterogeneities and the dispersion affect the image. In fact, in the situation with a strong source chirp signal the main effect of the medium heterogeneities is to introduce random phase distortions in the SAR data. We carry out novel scaling analysis that gives a precise characterization of this canonical phase perturbation and how it affects image resolution and stability. The main effect of the phase perturbation is to reduce the azimuthal resolution and the signal-to-noise ratio and we quantify this performance degradation.

PACS numbers: 78A46, 78A48, 78M35

1. Introduction

In spaceborne Synthetic Aperture Radar (SAR) and for imaging or communication through the earth's ionosphere the signal is affected by small scale fluctuations in the index of refraction, these may for instance be associated with optical turbulence. Moreover, the signal will be affected by a dispersive effect of the plasma whose strength depends on the electron number density. As in [23] we model these effects and the atmospheric propagation via the Klein-Gordon equation parameterized in terms of a random index of refraction and a random Langmuir frequency. This frequency characterizes the frequency response of the total electron content of the ionosphere.

Starting with an assumed model for propagation in terms of a random phase correction the SAR image formation is analyzed in [17] in terms of resolution. In [15] an approach to compensate for the effects of the medium clutter is set forth by using data at several frequencies. These data can be used for explicit estimation and compensation of the random phase resulting from the medium clutter. In the so-called phase gradient autofocus (PGA) approach [24] one also uses redundancy in the observation of the phase in order to estimate it and compensate for it. Regarding specific schemes for compensation of atmospheric and ionospheric effects in SAR images we refer to [2, 19, 15] and references therein. To construct atmospheric and ionospheric mitigation schemes it is useful to have insight about how atmospheric and ionospheric heterogeneities affect the measurements and the SAR resolution and stability and this is the focus of our paper. Our point of view here is to push through an analytic discussion for how the propagated wave field can be described in a distinguished scaling limit. Here, the distinguished limit refers to the scale separation limit that reflects the typical physical scaling ratios in the SAR regime and for which we can give a general description of the quantities of interest via asymptotic analysis. We will show by a rigorous analysis how the propagation of the wave field through the randomly heterogeneous medium gives rise to random phase distortions. This gives a novel characterization of how the SAR data phase statistics relates to the statistics of the medium. A notable feature of our analysis is that we can give an explicit account for how the signal-to-noise ratio is affected depending of the relative size of the medium fluctuations. The other main parameter that affects this signal-to-noise ratio is the size of the aperture relative to the correlation range of the medium fluctuations. It is interesting to note that the signal-to-noise ratio is mostly affected in a mid range for this parameter ratio. For very small ratios the phase varies little with respect to source location on the array and thus gives only an image shift rather than a resolution degradation, while for very large ratios there is a self-averaging effect as the phase correction becomes uncorrelated on the different positions of the antenna. We remark that the SAR aperture will in practice be constrained by the beam width, the illumination geometry, of the SAR apparatus. The explicit link that we provide between medium statistics and SAR data perturbation is useful in order to understand and tune phase compensation techniques like PGA. In addition to the random phase correction in the SAR data affecting the azimuthal resolution there is

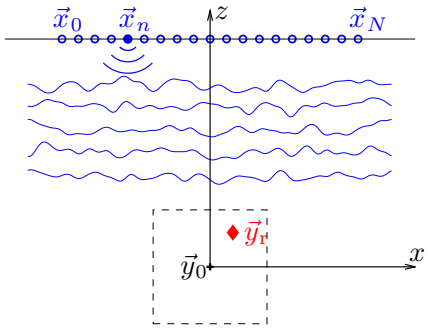

Figure 1. Schematic of the SAR configuration: $\vec{\boldsymbol{x}}_n = (x_n, 0, L)$ is the n-th position of the antenna, $\vec{\boldsymbol{y}}_r$ is the reflector position, and $\vec{\boldsymbol{y}}_0 = (0, 0, 0)$ is the center of the search area.

also an overall deterministic shift in the SAR image that is caused by a group delay associated with the deterministic part of the Langmuir frequency.

The outline of the papers is as follows. In Section 2 we review the basic SAR matched filter image formation procedure. Then we discuss the modeling and scaling assumptions that we use in Section 3. We carry out the multiscale analysis of the Green's function in Section 4 and use this to characterize the ambiguity function associated with the SAR image in Section 5. The analysis of the ambiguity function shows how resolution and stability are affected by medium clutter.

2. Matched filter processing

In the classical SAR setup, an antenna located on a satellite moves along a straight trajectory. At regularly spaced positions $\vec{\boldsymbol{x}}_n$, $n = 1, \ldots, N$ along this trajectory and at regularly spaced times nT, the antenna emits an electromagnetic pulse $s(t - nT)$ that is reflected by the reflectors present in the medium, and the scattered wave $R_n(t)$ is detected by the same antenna. The collection of received signals $(R_n(t))_{t,n}$ is then used to produce an image. Here the subscript in t, n refers to the fact that we regard the observations as a random field in these arguments. In this section we give a simple but accurate model that describes how the signals are produced and we also present the usual SAR imaging process.

The antenna can be a point source, or a slotted waveguide [10], or a microstrip antenna [21]. In this paper we carry out the analysis with a point source. The antenna moves along a straight trajectory, along the x-axis. The successive positions of the antenna are $\vec{\boldsymbol{x}}_n = (x_n, 0, L)$, $n = 1, \ldots, N$, with $x_n = (n/N - 1/2)D$ (see Figure 1). Throughout the paper we will use boldface vector notation $\vec{\boldsymbol{x}} = (x, y, z)$ to represent three-dimensional vectors, while we use boldface notation $\boldsymbol{x} = (x, y)$ to represent two-dimensional vectors for lateral spatial coordinates. The total length of the antenna

trajectory is D. The antenna at $\vec{\boldsymbol{x}}_n$ emits the signal $s(t-nT)$. The source signal is the chirped pulse

$$s(t) = \frac{1}{2}a\Big(\frac{t}{T_{\rm p}}\Big)\exp\,(\,-i\omega_{\rm c}t - i\pi\gamma t^2), \tag{1}$$

where $\omega_{\rm c}$ is the carrier (angular) frequency, γ is the chirp parameter, $a(t)$ is the normalized pulse shape function, and $T_{\rm p}$ is the pulse width. For instance, we may have $a(t)=\exp(-t^2)$ or $a(t)=\mathbf{1}_{[-1,1]}(t)$.

The antenna records the backscattered signal $R_n(t)$. A deramping is applied, that is, a multiplication by the opposite quadratic phase which recompresses the signal [4], so that we obtain the signals $S_n(t)$ defined by

$$S_n(t) = \exp[i\omega_{\rm c}(t-nT-2\tau_0) + i\pi\gamma(t-nT-2\tau_0)^2]R_n(t), \tag{2}$$

where $\tau_0 = |\vec{\boldsymbol{x}}_{N/2} - \vec{\boldsymbol{y}}_0|/c_0$, c_0 is the reference background velocity, $\vec{\boldsymbol{y}}_0=(0,0,0)$ is the center of the search area, and $\vec{\boldsymbol{x}}_{N/2}=(0,0,L)$ is the center of the antenna trajectory (and therefore $\tau_0 = L/c_0$). The set of signals $S_n(t)$, $n=1,\dots,N$, is the SAR data set. We remark that the variable t is sometimes referred to as the "fast time" and the variable n as the "slow time" in the SAR literature. Moreover, centering with a fixed τ_0 that does not depend on n is sometimes referred to as strip map mode.

Let us assume that there is a single target in the medium, whose position is $\vec{\boldsymbol{y}}_{\rm r}$. This target acts as a point reflector. Using the Born approximation, the backscattered field measured at the antenna is [7]

$$\begin{aligned} R_n(t) &= \frac{\omega_{\rm c}^2}{2\pi}\int \hat{G}(\omega,\vec{\boldsymbol{x}}_n,\vec{\boldsymbol{y}}_{\rm r})v_{\rm r}\hat{G}(\omega,\vec{\boldsymbol{y}}_{\rm r},\vec{\boldsymbol{x}}_n)\hat{s}(\omega)\exp\,[\,-i\omega(t-nT)]d\omega \\ &= \frac{\omega_{\rm c}^2 v_{\rm r}}{2\pi}\int \hat{G}(\omega,\vec{\boldsymbol{x}}_n,\vec{\boldsymbol{y}}_{\rm r})^2\hat{s}(\omega)\exp\,[\,-i\omega(t-nT)]d\omega, \end{aligned} \tag{3}$$

where $v_{\rm r}$ is the reflectivity of the target reflector and we have used the reciprocity identity $\hat{G}(\omega,\vec{\boldsymbol{x}},\vec{\boldsymbol{y}}) = \hat{G}(\omega,\vec{\boldsymbol{y}},\vec{\boldsymbol{x}})$. In a three-dimensional homogeneous non-dispersive medium with constant background velocity c_0, the Green's function is

$$\hat{G}(\omega,\vec{\boldsymbol{x}},\vec{\boldsymbol{y}})\;|_{\rm homo} = \frac{1}{4\pi|\vec{\boldsymbol{x}}-\vec{\boldsymbol{y}}|}\exp\Big(i\frac{\omega}{c_0}|\vec{\boldsymbol{x}}-\vec{\boldsymbol{y}}|\Big).$$

Therefore, in the case in which there is a single target at $\vec{\boldsymbol{y}}_{\rm r}$ and the medium is homogeneous and non-dispersive, the recorded signal (after deramping) has the form

$$\begin{aligned} S_n(t)\;|_{\rm homo} \;&= \frac{\omega_{\rm c}^2 v_{\rm r}}{32\pi^2|\vec{\boldsymbol{y}}_{\rm r}-\vec{\boldsymbol{x}}_n|^2}a\Big(\frac{t-nT}{T_{\rm p}} - 2\frac{|\vec{\boldsymbol{x}}_n-\vec{\boldsymbol{y}}_{\rm r}|}{c_0T_{\rm p}}\Big)\exp\Big[2i\omega_{\rm c}(\frac{|\vec{\boldsymbol{x}}_n-\vec{\boldsymbol{y}}_{\rm r}|}{c_0}-\tau_0)\Big] \\ &\quad\times\exp\Big[4i\pi\gamma(t-nT-2\tau_0)(\frac{|\vec{\boldsymbol{x}}_n-\vec{\boldsymbol{y}}_{\rm r}|}{c_0}-\tau_0) - 4i\pi\gamma(\frac{|\vec{\boldsymbol{x}}_n-\vec{\boldsymbol{y}}_{\rm r}|}{c_0}-\tau_0)^2\Big], \end{aligned}$$

and in the Fourier domain

$$\hat{S}_n(\omega)\;|_{\rm homo} = \omega_{\rm c}^2 v_{\rm r}\hat{H}(\omega,\vec{\boldsymbol{x}}_n,\vec{\boldsymbol{y}}_{\rm r})\exp(i\omega(nT+2\tau_0)), \tag{4}$$

where we have defined

$$\begin{aligned} \hat{H}(\omega,\vec{\boldsymbol{x}},\vec{\boldsymbol{y}}) &= \frac{T_{\rm p}}{32\pi^2|\vec{\boldsymbol{y}}-\vec{\boldsymbol{x}}|^2}\hat{a}\Big[T_{\rm p}\Big(4\pi\gamma(\frac{|\vec{\boldsymbol{x}}-\vec{\boldsymbol{y}}|}{c_0}-\tau_0)+\omega\Big)\Big]\exp\Big[2i\omega_{\rm c}(\frac{|\vec{\boldsymbol{x}}-\vec{\boldsymbol{y}}|}{c_0}-\tau_0)\Big] \\ &\quad\times\exp\Big[2i\omega(\frac{|\vec{\boldsymbol{x}}-\vec{\boldsymbol{y}}|}{c_0}-\tau_0)+4i\pi\gamma(\frac{|\vec{\boldsymbol{x}}-\vec{\boldsymbol{y}}|}{c_0}-\tau_0)^2\Big]. \end{aligned} \tag{5}$$

Note that
- the support of the function $\hat{H}(\omega, \vec{\boldsymbol{x}}, \vec{\boldsymbol{y}})$ is concentrated around $|\vec{\boldsymbol{x}} - \vec{\boldsymbol{y}}| \simeq c_0(\tau_0 - \frac{\omega}{4\pi\gamma})$ (this property gives the range resolution, as we will see below in Section 5.1)
- if $\omega_{\rm c} \gg \pi\gamma T_{\rm p}$, then the phase varies more rapidly than the amplitude (this property gives the azimuthal resolution, as we will see below in Section 5.2).

In general, the medium is not known and the SAR matched filter (or adjoint method) is the point spread function [7, 8]

$$\begin{aligned} I_n(\vec{\boldsymbol{y}}_{\rm s}) = & \int \overline{H}(t - nT - 2\tau_0, \vec{\boldsymbol{x}}_n, \vec{\boldsymbol{y}}_{\rm s}) S_n(t) dt \\ = & \frac{1}{2\pi} \int \overline{\hat{H}}(\omega, \vec{\boldsymbol{x}}_n, \vec{\boldsymbol{y}}_{\rm s}) \exp(-i\omega(nT + 2\tau_0)) \hat{S}_n(\omega) d\omega, \end{aligned} \tag{6}$$

where $\bar{\cdot}$ stands for complex conjugation. The point spread function matches the received signal S_n against the synthetic signal H that should be the one corresponding to the situation in which there is a point reflector at the search point $\vec{\boldsymbol{y}}_{\rm s}$ and the medium is homogeneous with background velocity c_0. It is the optimal filter in the sense of providing the best signal-to-noise ratio in the presence of additive white noise [7, 8]. In SAR the point spread function is summed over n, which gives the ambiguity function of the SAR system that we define in our paper by

$$\mathcal{I}(\vec{\boldsymbol{y}}_{\rm s}) = \Big| \sum_{n=1}^{N} I_n(\vec{\boldsymbol{y}}_{\rm s}) \Big|^2. \tag{7}$$

As we shall see in the following, this imaging functional produces high-resolution images and it is possible to quantify its performance in terms of resolution and signal-to-noise ratio when the SAR data are collected in a randomly heterogeneous and dispersive medium.

3. Modeling and scaling assumptions for the wave equation

The medium in which the waves propagate is heterogeneous and dispersive. The wave equation is the Klein-Gordon equation

$$\frac{n^2(\vec{\boldsymbol{x}})}{c_0^2} E_{tt} - \Delta E + \frac{\omega_{\rm pe}^2(\vec{\boldsymbol{x}})}{c_0^2} E = s(t)\delta(\vec{\boldsymbol{x}} - \vec{\boldsymbol{y}}_{\rm s}), \tag{8}$$

where c_0 is the light velocity in the homogeneous background medium, $\omega_{\rm pe}$ is the Langmuir (or plasma electronic) frequency (depending on the local electron density), and n is the index of refraction. We use the notation E_{tt} for the second-order partial with respect to time and ΔE is the spatial Laplacian. Here we have assumed a point source at $\vec{\boldsymbol{y}}_{\rm s}$ emitting the signal $s(t)$ given by (1).

The coefficients of the equation $\omega_{\rm pe}(\vec{\boldsymbol{x}})$ and $n(\vec{\boldsymbol{x}})$ are spatially varying and we model them to have the form

$$\omega_{\rm pe}^2(\vec{\boldsymbol{x}}) = \omega_0^2 \Big(1 + \sigma_\nu \nu(\frac{\vec{\boldsymbol{x}}}{\ell_\nu})\Big), \tag{9}$$

$$n^2(\vec{\boldsymbol{x}}) \ = 1 + \sigma_\mu \mu(\frac{\vec{\boldsymbol{x}}}{\ell_\mu}), \tag{10}$$

where ω_0 is the central Langmuir frequency (corresponding to the average electron density), and ν and μ are two stationary random processes with mean zero and ergodic properties. They are normalized so that their standard deviations and correlation lengths are of order one. The random process ν describes the fluctuations of the Langmuir frequency (due to the fluctuations of the electron density), whose typical relative amplitude is σ_ν and correlation length is ℓ_ν. Similarly the random process μ describes the fluctuations of the index of refraction, whose typical relative amplitude is σ_μ and correlation length is ℓ_μ. The fluctuations of the Langmuir frequency give rise to random dispersive effects. The fluctuations of the index of refraction give rise to random scattering effects. We will describe these effects in the next sections.

In this paper we set forth a multiscale approach to analyze the resolution and stability of the SAR imaging functional. This multiscale approach is based on the typical orders of magnitudes for the different quantities that play a role and it will give a comprehensive description of the wave propagation in the SAR regime. It is an extension of the results obtained in [14] in a different regime.

The typical numbers that can be found in the literature are [23]:
- carrier frequency $\omega_{\rm c}$ of the order of 10^9 Hz.
- bandwidth $B = 2\pi\gamma T_{\rm p}$ of the order of 10^7 Hz.
- pulse width $T_{\rm p}$ of the order of $5\,10^{-5}$ s, which gives $\omega_{\rm p} = 2\pi/T_{\rm p}$ of the order of 10^5 Hz.
- Langmuir frequency ω_0 of the order of 10^7 Hz.
- propagation distance L (round trip from the satellite to the ground): 1600 km, which corresponds to a frequency $\omega_L = 2\pi c_0/L$ of the order of 10^3 Hz.

Based on these values, we can introduce a small dimensionless parameter ε^2 (of the order of 10^{-2}) such that the ratios between the different characteristic parameters obey the scaling relations:

$$\frac{\omega_{\rm c}}{\omega_L} \sim \varepsilon^{-6}, \qquad \frac{B}{\omega_L} \sim \frac{\omega_0}{\omega_L} \sim \varepsilon^{-4}, \qquad \frac{\omega_{\rm p}}{\omega_L} \sim \varepsilon^{-2}. \tag{11}$$

We will here consider the scaling limit $\varepsilon \to 0$. Physically it means that we consider a regime of separation of scales as indicated above. In our paper we discuss the simplification that follows in such a scaling regime by deriving an asymptotic approximation for the quantities of interest in the SAR configuration.

We need also to specify the characteristic parameters of the random fluctuations. From [1, 3] the electron density fluctuates in the ionosphere with a correlation radius ℓ_ν of the order of 10 km, which corresponds to a frequency $\omega_\nu = \frac{2\pi c_0}{\ell_\nu} = 10^5$ Hz, and with a typical relative amplitude of the order of 10%. Therefore we have

$$\sigma_\nu \sim \varepsilon, \qquad \frac{\omega_\nu}{\omega_L} \sim \varepsilon^{-2}. \tag{12}$$

We will consider fluctuations of the index of refraction with a correlation radius ℓ_μ of the same order as the one of the electron density. The forthcoming analysis will show that the effect of the fluctuations of the index of refraction are comparable to those of the electron density when their typical amplitude is much smaller than the one of the

electron density. More precisely we will assume that they are of order 10^{-5} (or smaller). Therefore we have

$$\sigma_\mu \sim \varepsilon^5, \qquad \frac{\omega_\mu}{\omega_L} \sim \varepsilon^{-2}. \tag{13}$$

Such small fluctuations of the index of refraction are in fact typical in the atmosphere [22, Chapter 2]. We stress here the above parameters are chosen as representing a possible scaling scenario. In this scaling scenario random dispersive effects and random scattering effects interact at a comparable level. If for instance σ_μ happens to be much smaller in a considered situation, then we can indeed ignore the random scattering term. However, here we consider the most delicate situation where both effects are present and at a comparable level.

Finally we consider that the total length of the antenna trajectory D is of the order of a few tens of kilometers, which corresponds to a frequency $\omega_D = \frac{2\pi c_0}{D}$ of the order of 10^5 Hz, and we look for the reflector around the central position $\vec{\boldsymbol{y}}_0 = (0,0,0)$ in a search window (for the search point $\vec{\boldsymbol{y}}_{\rm s}$) of the order of 10-100 meters, which corresponds to a frequency $\omega_{\boldsymbol{y}_{\rm s}} = 2\pi c_0/|\vec{\boldsymbol{y}}_{\rm s}|$ of the order of 10^7 Hz. Therefore we have

$$\frac{\omega_D}{\omega_L} \sim \varepsilon^{-2}, \qquad \frac{\omega_{\boldsymbol{y}_{\rm s}}}{\omega_L} \sim \varepsilon^{-4}. \tag{14}$$

We now formulate the wave problem in the scaling regime described above. We consider the scaled version of the wave equation, expressed in terms of the small parameter ε and otherwise dimensionless parameters of order one where we retain the parameter notation from our above discussion (with some abuse of notation):

$$\frac{1}{c_0^2}\Big(1+\varepsilon^5\mu(\frac{\vec{\boldsymbol{x}}}{\varepsilon^2})\Big)E^\varepsilon_{tt} - \Delta E^\varepsilon + \frac{\omega_0^2}{\varepsilon^8 c_0^2}\Big(1+\varepsilon\nu(\frac{\vec{\boldsymbol{x}}}{\varepsilon^2})\Big)E^\varepsilon = s^\varepsilon(t)\delta(\vec{\boldsymbol{x}} - \vec{\boldsymbol{y}}^\varepsilon_{\rm s}), \tag{15}$$

corresponding to the distance and travel time from the array to the scatterer being of order one in these non-dimensionalized scaling with ε now giving relative scaling relations. That is in Eq. (8) we normalize units by this reference time and this reference length, to get quantities scaled by ε according to the above scaling discussion, however, retain the parameter symbols from above to retain the interpretation of what the parameters represent. Here we also assume that the source is localized at the point $\vec{\boldsymbol{y}}^\varepsilon_{\rm s}$ and emits the source pulse:

$$s^\varepsilon(t) = \frac{1}{2}a\Big(\frac{t}{\varepsilon^2 T_{\rm p}}\Big)\exp\Big(-i\frac{\omega_{\rm c}}{\varepsilon^6}t - i\pi\frac{\gamma}{\varepsilon^6}t^2\Big), \tag{16}$$

where the scaling of the last term by ε^{-6} follows from the magnitude of the bandwidth given above. We introduce the scaled Fourier transform:

$$\hat{s}^\varepsilon(\omega) = \int s^\varepsilon(t)\exp\Big(i(\frac{\omega_{\rm c}}{\varepsilon^6} + \frac{\omega}{\varepsilon^4})t\Big)dt, \tag{17}$$

which is the usual Fourier transform but evaluated at the frequency $\frac{\omega_{\rm c}}{\varepsilon^6} + \frac{\omega}{\varepsilon^4}$. The particular scaled and shifted Fourier transform is determined by the form of the source,

whose spectrum is concentrated around the carrier frequency $\omega_{\rm c}/\varepsilon^6$ with a bandwidth of the order of ε^{-4}, as can be seen from the limit (obtained by a stationary phase argument)

$$\lim_{\varepsilon\to 0}\varepsilon^{-3}\hat{s}^\varepsilon(\omega)=\frac{e^{-i\pi/4}}{2\sqrt{\gamma}}a\Big(\frac{\omega}{2\pi\gamma T_{\rm p}}\Big). \tag{18}$$

By taking the scaled Fourier transform of the wave equation we get the Helmholtz equation:

$$\Delta\hat{E}^\varepsilon+\Big[\frac{1}{c_0^2}\Big(\frac{\omega_{\rm c}}{\varepsilon^6}+\frac{\omega}{\varepsilon^4}\Big)^2\Big(1+\varepsilon^5\mu(\frac{\vec{\boldsymbol{x}}}{\varepsilon^2})\Big)-\frac{\omega_0^2}{\varepsilon^8c_0^2}\Big(1+\varepsilon\nu(\frac{\vec{\boldsymbol{x}}}{\varepsilon^2})\Big)\Big]\hat{E}^\varepsilon=-\hat{s}^\varepsilon(\omega)\delta(\vec{\boldsymbol{x}}-\vec{\boldsymbol{y}}_{\rm s}^\varepsilon). \tag{19}$$

According to (14), the antenna position is of the form

$$\vec{\boldsymbol{x}}_n^\varepsilon=(\varepsilon^2\boldsymbol{x}_n,L),$$

and the reflector and the search point are of the form

$$\vec{\boldsymbol{y}}_{\rm r}^\varepsilon=\varepsilon^4(\boldsymbol{y}_{\rm r},z_{\rm r}),\qquad \vec{\boldsymbol{y}}_{\rm s}^\varepsilon=\varepsilon^4(\boldsymbol{y}_{\rm s},z_{\rm s}).$$

As discussed in Section 2 we would like to identify the Green's function from $\vec{\boldsymbol{y}}_{\rm s}^\varepsilon$ or $\vec{\boldsymbol{y}}_{\rm r}^\varepsilon$ to $\vec{\boldsymbol{x}}_n^\varepsilon$ in order to characterize the SAR data. This Green's function should be identified for a frequency in the spectrum of the source signal, that is, for a frequency of the form $\frac{\omega_{\rm c}}{\varepsilon^6}+\frac{\omega}{\varepsilon^4}$.

4. Multiscale analysis of the Green's function

The Green's function $\hat{G}^\varepsilon(\omega,\vec{\boldsymbol{x}};\vec{\boldsymbol{y}}_{\rm s}^\varepsilon)$ from the point $\vec{\boldsymbol{y}}_{\rm s}^\varepsilon=\varepsilon^4\vec{\boldsymbol{y}}_{\rm s}=\varepsilon^4(\boldsymbol{y}_{\rm s},z_{\rm s})$ to a point $\vec{\boldsymbol{x}}=(\boldsymbol{x},z)$ at the frequency $\frac{\omega_{\rm c}}{\varepsilon^6}+\frac{\omega}{\varepsilon^4}$ is the solution of the Helmholtz equation (19) with $\hat{s}^\varepsilon(\omega)=1$ and $\vec{\boldsymbol{y}}_{\rm s}^\varepsilon=\varepsilon^4\vec{\boldsymbol{y}}_{\rm s}$. This equation can be written as

$$\Delta\hat{G}^\varepsilon+{q_\omega^\varepsilon}^2\hat{G}^\varepsilon+\frac{1}{\varepsilon^7}Q(\frac{\vec{\boldsymbol{x}}}{\varepsilon^2})\hat{G}^\varepsilon+\frac{2\omega_{\rm c}\omega}{c_0^2\varepsilon^5}\mu(\frac{\vec{\boldsymbol{x}}}{\varepsilon^2})\hat{G}^\varepsilon+\frac{\omega^2}{c_0^2\varepsilon^3}\mu(\frac{\vec{\boldsymbol{x}}}{\varepsilon^2})\hat{G}^\varepsilon=-\delta(\vec{\boldsymbol{x}}-\varepsilon^4\vec{\boldsymbol{y}}_{\rm s}), \tag{20}$$

where the effective wavenumber q_ω^ε is defined by

$${q_\omega^\varepsilon}^2=\frac{1}{c_0^2}\Big(\frac{\omega_{\rm c}}{\varepsilon^6}+\frac{\omega}{\varepsilon^4}\Big)^2-\frac{\omega_0^2}{c_0^2\varepsilon^8}, \tag{21}$$

and the zero-mean random process Q is

$$Q(\vec{\boldsymbol{x}})=\frac{\omega_{\rm c}^2}{c_0^2}\mu(\vec{\boldsymbol{x}})-\frac{\omega_0^2}{c_0^2}\nu(\vec{\boldsymbol{x}}). \tag{22}$$

We introduce the scaled space-time Fourier transform:

$$\check{G}^\varepsilon(\omega,\boldsymbol{k},z;\vec{\boldsymbol{y}}_{\rm s}^\varepsilon)=\int_{\mathbb{R}^2}\hat{G}^\varepsilon(\omega,\boldsymbol{x},z;\vec{\boldsymbol{y}}_{\rm s}^\varepsilon)\exp\Big(i\boldsymbol{k}\cdot\frac{\boldsymbol{x}}{\varepsilon^4}\Big)d\boldsymbol{x}. \tag{23}$$

By taking the space-time Fourier transform of the wave equation we find

$$\begin{aligned}&\frac{\partial^2\check{G}^\varepsilon}{\partial z^2}(\boldsymbol{k})+{q_{\omega,\boldsymbol{k}}^\varepsilon}^2\check{G}^\varepsilon(\boldsymbol{k})\\&=-\delta(z-\varepsilon^4z_{\rm s})\exp\left(i\boldsymbol{k}\cdot\boldsymbol{y}_{\rm s}\right)-\frac{1}{\varepsilon^7(2\pi)^2}\int\check{Q}\Big(\boldsymbol{k}',\frac{z}{\varepsilon^2}\Big)\check{G}^\varepsilon(\boldsymbol{k}-\varepsilon^2\boldsymbol{k}')d\boldsymbol{k}'\\&-\frac{2\omega\omega_{\rm c}}{\varepsilon^5c_0^2(2\pi)^2}\int\check{\mu}\Big(\boldsymbol{k}',\frac{z}{\varepsilon^2}\Big)\check{G}^\varepsilon(\boldsymbol{k}-\varepsilon^2\boldsymbol{k}')d\boldsymbol{k}'-\frac{\omega^2}{\varepsilon^3c_0^2(2\pi)^2}\int\check{\mu}\Big(\boldsymbol{k}',\frac{z}{\varepsilon^2}\Big)\check{G}^\varepsilon(\boldsymbol{k}-\varepsilon^2\boldsymbol{k}')d\boldsymbol{k}',\end{aligned} \tag{24}$$

where the effective wavenumber $q^\varepsilon_{\omega,\boldsymbol{k}}$ is given by

$$\big(q^\varepsilon_{\omega,\boldsymbol{k}}\big)^2 = \frac{1}{c_0^2}\Big[\Big(\frac{\omega_{\rm c}}{\varepsilon^6}+\frac{\omega}{\varepsilon^4}\Big)^2 - \frac{\omega_0^2}{\varepsilon^8}\Big] - \frac{|\boldsymbol{k}|^2}{\varepsilon^8}, \tag{25}$$

and $\check{Q}$ is the unscaled Fourier transform of Q:

$$\check{Q}(\boldsymbol{k},z) = \int_{\mathbb{R}^2} Q(\boldsymbol{x},z)\exp\left(i\boldsymbol{k}\cdot\boldsymbol{x}\right)d\boldsymbol{x}.$$

We next decompose the wave field into an upgoing and and downgoing wave modes whose complex amplitudes are denoted by $\check{A}^\varepsilon$ and $\check{B}^\varepsilon$ respectively and are defined by:

$$\check{A}^\varepsilon(\omega,\boldsymbol{k},z;\vec{\boldsymbol{y}}^\varepsilon_{\rm s}) = \Big[\frac{1}{2}\check{G}^\varepsilon(\omega,\boldsymbol{k},z;\vec{\boldsymbol{y}}^\varepsilon_{\rm s}) + \frac{1}{2iq^\varepsilon_{\omega,\boldsymbol{k}}}\frac{\partial\check{G}^\varepsilon}{\partial z}(\omega,\boldsymbol{k},z;\vec{\boldsymbol{y}}^\varepsilon_{\rm s})\Big]\exp\left(-iq^\varepsilon_{\omega,\boldsymbol{k}}z\right),$$

$$\check{B}^\varepsilon(\omega,\boldsymbol{k},z;\vec{\boldsymbol{y}}^\varepsilon_{\rm s}) = \Big[\frac{1}{2}\check{G}^\varepsilon(\omega,\boldsymbol{k},z;\vec{\boldsymbol{y}}^\varepsilon_{\rm s}) - \frac{1}{2iq^\varepsilon_{\omega,\boldsymbol{k}}}\frac{\partial\check{G}^\varepsilon}{\partial z}(\omega,\boldsymbol{k},z;\vec{\boldsymbol{y}}^\varepsilon_{\rm s})\Big]\exp\left(iq^\varepsilon_{\omega,\boldsymbol{k}}z\right).$$

Here, with "upgoing" we mean propagation in the positive z-direction. The decomposition then reads

$$\check{G}^\varepsilon(\omega,\boldsymbol{k},z;\vec{\boldsymbol{y}}^\varepsilon_{\rm s}) = \check{A}^\varepsilon(\omega,\boldsymbol{k},z;\vec{\boldsymbol{y}}^\varepsilon_{\rm s})\exp\left(iq^\varepsilon_{\omega,\boldsymbol{k}}z\right) + \check{B}^\varepsilon(\omega,\boldsymbol{k},z;\vec{\boldsymbol{y}}^\varepsilon_{\rm s})\exp\left(-iq^\varepsilon_{\omega,\boldsymbol{k}}z\right), \tag{26}$$

and it then follows that the mode amplitudes satisfy

$$\frac{\partial\check{A}^\varepsilon}{\partial z}(\omega,\boldsymbol{k},z;\vec{\boldsymbol{y}}^\varepsilon_{\rm s})\exp\left(iq^\varepsilon_{\omega,\boldsymbol{k}}z\right) + \frac{\partial\check{B}^\varepsilon}{\partial z}(\omega,\boldsymbol{k},z;\vec{\boldsymbol{y}}^\varepsilon_{\rm s})\exp\left(-iq^\varepsilon_{\omega,\boldsymbol{k}}z\right) = 0.$$

Substituting into (24) we find the coupled system of equations that governs the evolution of the wave mode amplitudes:

$$\begin{aligned}\frac{\partial\check{A}^\varepsilon}{\partial z}(\boldsymbol{k}) = \frac{i}{q^\varepsilon_{\omega,\boldsymbol{k}}\varepsilon^7 2(2\pi)^2}\int\check{Q}\Big(\boldsymbol{k}',\frac{z}{\varepsilon^2}\Big)\Big[\check{A}^\varepsilon(\boldsymbol{k}-\varepsilon^2\boldsymbol{k}')\exp\Big(i(q^\varepsilon_{\omega,\boldsymbol{k}-\varepsilon^2\boldsymbol{k}'}-q^\varepsilon_{\omega,\boldsymbol{k}})z\Big)\\ + \check{B}^\varepsilon(\boldsymbol{k}-\varepsilon^2\boldsymbol{k}')\exp\Big(i(-q^\varepsilon_{\omega,\boldsymbol{k}-\varepsilon^2\boldsymbol{k}'}-q^\varepsilon_{\omega,\boldsymbol{k}})z\Big)\Big]d\boldsymbol{k}',\end{aligned} \tag{27}$$

$$\begin{aligned}\frac{\partial\check{B}^\varepsilon}{\partial z}(\boldsymbol{k}) = -\frac{i}{q^\varepsilon_{\omega,\boldsymbol{k}}\varepsilon^7 2(2\pi)^2}\int\check{Q}\Big(\boldsymbol{k}',\frac{z}{\varepsilon^2}\Big)\Big[\check{A}^\varepsilon(\boldsymbol{k}-\varepsilon^2\boldsymbol{k}')\exp\Big(i(q^\varepsilon_{\omega,\boldsymbol{k}-\varepsilon^2\boldsymbol{k}'}+q^\varepsilon_{\omega,\boldsymbol{k}})z\Big)\\ + \check{B}^\varepsilon(\boldsymbol{k}-\varepsilon^2\boldsymbol{k}')\exp\Big(i(-q^\varepsilon_{\omega,\boldsymbol{k}-\varepsilon^2\boldsymbol{k}'}+q^\varepsilon_{\omega,\boldsymbol{k}})z\Big)\Big]d\boldsymbol{k}'.\end{aligned} \tag{28}$$

Here we have not written the last two terms that appear at the end of Eq (24) because they turn out to be negligible (this can be guessed because $1/(\varepsilon^5 q^\varepsilon_{\omega,\boldsymbol{k}}) = O(\varepsilon)$).

The system (27-28) is complemented by the radiation conditions that mean that no wave is incoming from infinity:

$$\check{A}^\varepsilon(\omega,\boldsymbol{k},z<\varepsilon^4 z_{\rm s};\vec{\boldsymbol{y}}^\varepsilon_{\rm s}) = 0, \qquad \check{B}^\varepsilon(\omega,\boldsymbol{k},z>L;\vec{\boldsymbol{y}}^\varepsilon_{\rm s}) = 0, \tag{29}$$

because the medium is homogeneous outside the region $z\in(0,L)$. We also have the jump condition at $z=\varepsilon^4 z_{\rm s}$:

$$\check{A}^\varepsilon(\omega,\boldsymbol{k},\varepsilon^4 z_{\rm s}^+;\vec{\boldsymbol{y}}^\varepsilon_{\rm s}) - \check{A}^\varepsilon(\omega,\boldsymbol{k},\varepsilon^4 z_{\rm s}^-;\vec{\boldsymbol{y}}^\varepsilon_{\rm s}) = \frac{i}{2q^\varepsilon_{\omega,\boldsymbol{k}}}\exp\left(-i\varepsilon^4 q^\varepsilon_{\omega,\boldsymbol{k}}z_{\rm s} + i\boldsymbol{k}\cdot\boldsymbol{y}_{\rm s}\right),$$

which gives with the radiation condition:

$$\check{A}^\varepsilon(\omega,\boldsymbol{k},\varepsilon^4 z_{\rm s}^+;\vec{\boldsymbol{y}}_{\rm s}^\varepsilon)=\frac{i}{2q^\varepsilon_{\omega,\boldsymbol{k}}}\exp\big(-i\varepsilon^4 q^\varepsilon_{\omega,\boldsymbol{k}} z_{\rm s}+i\boldsymbol{k}\cdot\boldsymbol{y}_{\rm s}\big). \tag{30}$$

We remark that, as we show below, the field reflected from the random heterogeneities of the medium are small and we do not give the jump condition for the down-propagating field $\check{B}^\varepsilon$.

We now carry out the asymptotic analysis.

1) We have

$$\begin{aligned}
\frac{1}{\varepsilon^7 q^\varepsilon_{\omega,\boldsymbol{k}}} &= \frac{c_0}{\omega_{\rm c}\varepsilon}+O(\varepsilon),\\
q^\varepsilon_{\omega,\boldsymbol{k}-\varepsilon^2\boldsymbol{k}'}+q^\varepsilon_{\omega,\boldsymbol{k}} &= \frac{2\omega_{\rm c}}{\varepsilon^6 c_0}+O(\varepsilon^{-4}),\\
q^\varepsilon_{\omega,\boldsymbol{k}-\varepsilon^2\boldsymbol{k}'}-q^\varepsilon_{\omega,\boldsymbol{k}} &= \frac{c_0\boldsymbol{k}\cdot\boldsymbol{k}'}{\omega_{\rm c}}+O(\varepsilon^2).
\end{aligned}$$

The first expansion allows us to simplify the multiplicative factors in the right-hand sides of the evolutions equations (27-28). The second expansion gives rapid phases that average out the crossed terms between the up-going and down-going wave mode amplitudes. The third expansion gives a simple form for the evolution equation of the up-going wave mode amplitude:

$$\frac{\partial\check{A}^\varepsilon}{\partial z}(\boldsymbol{k})=\frac{ic_0}{2(2\pi)^2\omega_{\rm c}\varepsilon}\int\check{Q}\Big(\boldsymbol{k}',\frac{z}{\varepsilon^2}\Big)\check{A}^\varepsilon(\boldsymbol{k}-\varepsilon^2\boldsymbol{k}')\exp\Big(i\frac{c_0\boldsymbol{k}\cdot\boldsymbol{k}'}{\omega_{\rm c}}z\Big)d\boldsymbol{k}'. \tag{31}$$

A similar equation is obtained for the down-going wave mode amplitude:

$$\frac{\partial\check{B}^\varepsilon}{\partial z}(\boldsymbol{k})=-\frac{ic_0}{2(2\pi)^2\omega_{\rm c}\varepsilon}\int\check{Q}\Big(\boldsymbol{k}',\frac{z}{\varepsilon^2}\Big)\check{B}^\varepsilon(\boldsymbol{k}-\varepsilon^2\boldsymbol{k}')\exp\Big(-i\frac{c_0\boldsymbol{k}\cdot\boldsymbol{k}'}{\omega_{\rm c}}z\Big)d\boldsymbol{k}'. \tag{32}$$

2) We have

$$\varepsilon^4 q^\varepsilon_{\omega,\boldsymbol{k}}=\frac{\omega_{\rm c}}{c_0\varepsilon^2}+\frac{\omega}{c_0}+O(\varepsilon^2).$$

This expansion allows us to simplify the initial condition (30) for $\check{A}^\varepsilon$:

$$\check{A}^\varepsilon(\omega,\boldsymbol{k},\varepsilon^4 z_{\rm s}^+;\vec{\boldsymbol{y}}_{\rm s}^\varepsilon)=\frac{ic_0\varepsilon^6}{2\omega_{\rm c}}\exp\Big(-i\frac{\omega_{\rm c}}{c_0\varepsilon^2}z_{\rm s}-i\frac{\omega}{c_0}z_{\rm s}+i\boldsymbol{k}\cdot\boldsymbol{y}_{\rm s}\Big). \tag{33}$$

Note that the initial wave mode amplitude has no rapid variation in $\boldsymbol{k}$, and the evolution equation (31) does not give rise to such rapid variation either, so we can simplify (31) into

$$\begin{aligned}
\frac{\partial\check{A}^\varepsilon}{\partial z}(\boldsymbol{k}) &= \frac{ic_0}{2(2\pi)^2\omega_{\rm c}\varepsilon}\int\check{Q}\Big(\boldsymbol{k}',\frac{z}{\varepsilon^2}\Big)\check{A}^\varepsilon(\boldsymbol{k})\exp\Big(i\frac{c_0\boldsymbol{k}\cdot\boldsymbol{k}'}{\omega_{\rm c}}z\Big)d\boldsymbol{k}'\\
&= \frac{ic_0}{2\omega_{\rm c}\varepsilon}Q\Big(-\frac{c_0\boldsymbol{k}}{\omega_{\rm c}}z,\frac{z}{\varepsilon^2}\Big)\check{A}^\varepsilon(\boldsymbol{k}).
\end{aligned} \tag{34}$$

This equation can be integrated and we find (to leading order):

$$\check{A}^\varepsilon(\omega,\boldsymbol{k},z;\vec{\boldsymbol{y}}_{\rm s}^\varepsilon)=\check{A}^\varepsilon(\omega,\boldsymbol{k},\varepsilon^4 z_{\rm s}^+;\vec{\boldsymbol{y}}_{\rm s}^\varepsilon)\exp\Big[\frac{ic_0}{2\omega_{\rm c}\varepsilon}\int_0^z Q\Big(-\frac{c_0\boldsymbol{k}}{\omega_{\rm c}}z',\frac{z'}{\varepsilon^2}\Big)dz'\Big], \tag{35}$$

for $z \in (\varepsilon^4 z_{\rm s}, L]$. Note that the random phase is of order one as $\varepsilon \to 0$ by a classical diffusion approximation argument and that it is smooth in $\boldsymbol{k}$.

Using the evolution equation (32) for $\check{B}^\varepsilon$ and the boundary condition (29) for $\check{B}^\varepsilon$ at $z = L$, we find that

$$\check{B}^\varepsilon(\omega, \boldsymbol{k}, z; \vec{\boldsymbol{y}}_{\rm s}^\varepsilon) = 0, \tag{36}$$

for $z \in (\varepsilon^4 z_{\rm s}, L]$. Indeed this corresponds to no wave energy coming in from $z = +\infty$.

3) We have

$$q^\varepsilon_{\omega,\boldsymbol{k}} = q^\varepsilon_\omega - \frac{|\boldsymbol{k}|^2 c_0}{2\varepsilon^2 \omega_{\rm c}} + \frac{|\boldsymbol{k}|^2 c_0 \omega}{2\omega_{\rm c}^2} + O(\varepsilon^2).$$

This gives that the Fourier transformed Green's function is of the form

$$\check{G}^\varepsilon(\omega, \boldsymbol{k}, z; \vec{\boldsymbol{y}}_{\rm s}^\varepsilon) = \check{A}^\varepsilon(\omega, \boldsymbol{k}, z; \vec{\boldsymbol{y}}_{\rm s}^\varepsilon) \exp\Big(- i\frac{|\boldsymbol{k}|^2 c_0 z}{2\varepsilon^2 \omega_{\rm c}} + i\frac{|\boldsymbol{k}|^2 c_0 \omega z}{2\omega_{\rm c}^2} + i q^\varepsilon_\omega z\Big), \tag{37}$$

for $z \in (\varepsilon^4 z_{\rm s}, L]$. Therefore at a point $\vec{\boldsymbol{x}} = (\varepsilon^2 \boldsymbol{x}_n, L)$ it is given by

$$\begin{aligned}
\hat{G}^\varepsilon(\omega, \varepsilon^2\boldsymbol{x}_n, L; \vec{\boldsymbol{y}}_{\rm s}^\varepsilon) &= \frac{1}{(2\pi)^2 \varepsilon^8} \int_{\mathbb{R}^2} \check{G}^\varepsilon(\omega, \boldsymbol{k}, L; \vec{\boldsymbol{y}}_{\rm s}^\varepsilon) \exp\Big(- i\frac{\boldsymbol{k}\cdot\boldsymbol{x}_n}{\varepsilon^2}\Big) d\boldsymbol{k} \\
&= \frac{1}{(2\pi)^2} \frac{i c_0}{2\omega_{\rm c}\varepsilon^2} \exp\Big(i q^\varepsilon_\omega L - i\frac{\omega_{\rm c}}{c_0 \varepsilon^2} z_{\rm s} - i\frac{\omega}{c_0} z_{\rm s}\Big) \\
&\quad \times \int \exp\Big[- \frac{i}{\varepsilon^2}\Big(\frac{|\boldsymbol{k}|^2 c_0 L}{2\omega_{\rm c}} + \boldsymbol{k}\cdot\boldsymbol{x}_n\Big) + i\Big(\frac{|\boldsymbol{k}|^2 c_0 \omega}{2\omega_{\rm c}^2} L + \boldsymbol{k}\cdot\boldsymbol{y}_{\rm s}\Big)\Big] \\
&\quad \times \exp\Big[\frac{i c_0}{2\omega_{\rm c}\varepsilon} \int_0^L Q\Big(- \frac{c_0 \boldsymbol{k}}{\omega_{\rm c}} z', \frac{z'}{\varepsilon^2}\Big) dz'\Big] d\boldsymbol{k}.
\end{aligned}$$

Note the presence of the rapid phase (of order ε^{-2}) in the $\boldsymbol{k}$-integral. By a stationary phase argument, the value of the integral is concentrated around an ε-neighborhood of the unique stationary point $\boldsymbol{k}_{st} = -\boldsymbol{x}_n \omega_{\rm c}/(c_0 L)$ and we find

$$\begin{aligned}
\hat{G}^\varepsilon(\omega, \varepsilon^2\boldsymbol{x}_n, L; \vec{\boldsymbol{y}}_{\rm s}^\varepsilon) &= \frac{1}{4\pi L} \exp\Big(i q^\varepsilon_\omega L - i\frac{\omega_{\rm c}}{c_0 \varepsilon^2} z_{\rm s} - i\frac{\omega}{c_0} z_{\rm s}\Big) \\
&\quad \times \exp\Big(i\frac{|\boldsymbol{x}_n|^2 \omega_{\rm c}}{2\varepsilon^2 c_0 L} + i\frac{|\boldsymbol{x}_n|^2 \omega}{2c_0 L} - i\omega_{\rm c}\frac{\boldsymbol{x}_n\cdot\boldsymbol{y}_{\rm s}}{c_0 L}\Big) \\
&\quad \times \exp\Big[\frac{i c_0}{2\omega_{\rm c}\varepsilon} \int_0^L Q\Big(\frac{\boldsymbol{x}_n}{L} z', \frac{z'}{\varepsilon^2}\Big) dz'\Big],
\end{aligned} \tag{38}$$

where q^ε_ω can be expanded as

$$q^\varepsilon_\omega = \frac{1}{c_0}\Big(\frac{\omega_{\rm c}}{\varepsilon^6} + \frac{\omega}{\varepsilon^4} - \frac{\omega_0^2}{2\varepsilon^2\omega_{\rm c}} + \frac{\omega\omega_0^2}{2\omega_{\rm c}^2} + O(\varepsilon^2)\Big). \tag{39}$$

Eq. (38) is the asymptotic expression of the Green's function that we will use in the next section for the analysis of the SAR imaging functional.

Note that the phase in (38) is nothing else but the expansion of

$$\frac{1}{c_0}\Big(\frac{\omega_{\rm c}}{\varepsilon^6} + \frac{\omega}{\varepsilon^4}\Big)|\varepsilon^4 \vec{\boldsymbol{y}}_{\rm s} - (\varepsilon^2 \boldsymbol{x}_n, L)|,$$

up to the deterministic phase ψ^ε_ω given by

$$\psi^\varepsilon_\omega = \frac{1}{c_0}\Big(- \frac{\omega_0^2}{2\varepsilon^2\omega_{\rm c}} + \frac{\omega\omega_0^2}{2\omega_{\rm c}^2}\Big)L, \tag{40}$$

which is due to the homogeneous Langmuir frequency ω_0, and the random phase $\phi^\varepsilon(\boldsymbol{x}_n)/2$ given by

$$\phi^\varepsilon(\boldsymbol{x}_n) = \frac{c_0}{\omega_{\rm c}\varepsilon}\int_0^L Q\Big(\frac{\boldsymbol{x}_n}{L}z', \frac{z'}{\varepsilon^2}\Big)dz', \tag{41}$$

which is due to the spatial fluctuations of the index of refraction and of the Langmuir frequency, over a path that to leading order is the straight line from the scatterer to the n-th antenna position $\vec{\boldsymbol{x}}^\varepsilon_n$. Therefore the random Green's function can be written in terms of the background non-dispersive Green's function as

$$\hat{G}^\varepsilon(\omega, \varepsilon^2\boldsymbol{x}_n, L; \vec{\boldsymbol{y}}^\varepsilon_{\rm s}) \qquad = \hat{G}^\varepsilon(\omega, \varepsilon^2\boldsymbol{x}_n, L; \vec{\boldsymbol{y}}^\varepsilon_{\rm s})\mid_{\rm homo} \exp\Big[\frac{i}{2}\phi^\varepsilon(\boldsymbol{x}_n) + i\psi^\varepsilon_\omega\Big], \tag{42}$$

$$\hat{G}^\varepsilon(\omega, \varepsilon^2\boldsymbol{x}_n, L; \vec{\boldsymbol{y}}^\varepsilon_{\rm s})\mid_{\rm homo} = \frac{1}{4\pi|(\varepsilon^2\boldsymbol{x}_n, L) - \vec{\boldsymbol{y}}^\varepsilon_{\rm s}|}\exp\Big[i(\frac{\omega_{\rm c}}{\varepsilon^6} + \frac{\omega}{\varepsilon^4})\frac{|(\varepsilon^2\boldsymbol{x}_n, L) - \vec{\boldsymbol{y}}^\varepsilon_{\rm s}|}{c_0}\Big]. \tag{43}$$

5. Multiscale analysis of the ambiguity function

Taking an inverse scaled Fourier transform, the signal received at the antenna position $\vec{\boldsymbol{x}}^\varepsilon_n = (\varepsilon^2\boldsymbol{x}_n, L)$ when there is a reflector at $\vec{\boldsymbol{y}}^\varepsilon_{\rm r} = \varepsilon^4\vec{\boldsymbol{y}}_{\rm r} = \varepsilon^4(\boldsymbol{y}_{\rm r}, z_{\rm r})$ is

$$R^\varepsilon_n(t) = \frac{\omega_{\rm c}^2 v_{\rm r}}{2\pi\varepsilon^{16}}\int \hat{G}^\varepsilon(\omega, \varepsilon^2\boldsymbol{x}_n, L; \vec{\boldsymbol{y}}^\varepsilon_{\rm r})^2\hat{s}^\varepsilon(\omega)\exp\Big[- i(\frac{\omega_{\rm c}}{\varepsilon^6} + \frac{\omega}{\varepsilon^4})(t - nT)\Big]d\omega, \tag{44}$$

where the source spectrum $\hat{s}^\varepsilon(\omega)$ is given by (17) and the Green's function by (38). The deramped signal is of the form

$$S^\varepsilon_n(t) = S^\varepsilon_n(t)\mid_{\rm homo}\exp\Big[- i\frac{\omega_0^2 L}{\varepsilon^2\omega_{\rm c}c_0} + i\phi^\varepsilon(\boldsymbol{x}_n)\Big]\exp\Big[i\frac{2\pi\gamma L}{\varepsilon^2 c_0}\frac{\omega_0^2}{\omega_{\rm c}^2}(t - nT - \frac{2L}{c_0})\Big], \tag{45}$$

where $S^\varepsilon_n(t)\mid_{\rm homo}$ is the signal that would have been obtained if the medium were homogeneous and non-dispersive:

$$S^\varepsilon_n(t)\mid_{\rm homo} = \frac{\omega_{\rm c}^2 v_{\rm r}}{\varepsilon^{12}}H^\varepsilon(t - nT - \frac{2L}{c_0}, \boldsymbol{x}_n, \vec{\boldsymbol{y}}_{\rm r}), \tag{46}$$

with

$$H^\varepsilon(t, \boldsymbol{x}_n, \vec{\boldsymbol{y}}_{\rm r}) = \frac{1}{32\pi^2L^2}\exp\Big[- 2i\frac{\omega_{\rm c}z_{\rm r}}{\varepsilon^2c_0} - 2i\frac{\omega_{\rm c}\boldsymbol{x}_n\cdot\boldsymbol{y}_{\rm r}}{c_0L} + i\frac{|\boldsymbol{x}_n|^2\omega_{\rm c}}{\varepsilon^2c_0L}\Big]$$
$$\times\exp\Big[- 2i\pi\frac{\gamma}{\varepsilon^2}t(\frac{2z_{\rm r}}{c_0} - \frac{|\boldsymbol{x}_n|^2}{c_0L})\Big]a\Big(\frac{t}{\varepsilon^2T_{\rm p}}\Big). \tag{47}$$

The point spread function at the search point $\vec{\boldsymbol{y}}^\varepsilon_{\rm s} = \varepsilon^4\vec{\boldsymbol{y}}_{\rm s} = \varepsilon^4(\boldsymbol{y}_{\rm s}, z_{\rm s})$ is

$$I_n(\vec{\boldsymbol{y}}^\varepsilon_{\rm s}) = \int\overline{H^\varepsilon}(t - nT - \frac{2L}{c_0}, \boldsymbol{x}_n, \vec{\boldsymbol{y}}_{\rm s})S^\varepsilon_n(t)dt,$$

where H^ε is given by (47) and the deramped recorded signal $S_n^\varepsilon(t)$ can be expressed in terms of the reflector at $\vec{\boldsymbol{y}}_{\rm r}^\varepsilon = \varepsilon^4(\boldsymbol{y}_{\rm r}, z_{\rm r})$ as (45). We find that

$$I_n(\vec{\boldsymbol{y}}_{\rm s}^\varepsilon) = \frac{\omega_{\rm c}^2 v_{\rm r} T_{\rm p}}{(32\pi^2 L^2)^2 \varepsilon^{10}} \exp\Big[2i\frac{\omega_{\rm c}}{c_0\varepsilon^2}(z_{\rm s}-z_{\rm r}) - i\frac{L\omega_0^2}{\varepsilon^2\omega_{\rm c}c_0}\Big] \\ \times \exp\Big[2i\frac{\omega_{\rm c}\boldsymbol{x}_n\cdot(\boldsymbol{y}_{\rm s}-\boldsymbol{y}_{\rm r})}{c_0 L} + i\phi^\varepsilon(\boldsymbol{x}_n)\Big] W_{\rm R}(z_{\rm s}; z_{\rm r}), \tag{48}$$

where we have defined

$$W_{\rm R}(z_{\rm s}; z_{\rm r}) = \mathcal{A}\Big(\frac{4\pi\gamma T_{\rm p}}{c_0}(z_{\rm s}-z_{\rm r}+\frac{L\omega_0^2}{2\omega_{\rm c}^2})\Big), \tag{49}$$

$$\mathcal{A}(\omega) \quad = \int |a(t)|^2 \exp(i\omega t)dt. \tag{50}$$

Finally the ambiguity function (7), up to a multiplicative factor (proportional to the reflectivity $v_{\rm r}$ of the reflector), can be written as

$$\mathcal{I}(\vec{\boldsymbol{y}}_{\rm s}^\varepsilon) = \Big|W_{\rm R}(z_{\rm s}; z_{\rm r})\Big|^2 \Big|W_{\rm A}(\boldsymbol{y}_{\rm s}; \boldsymbol{y}_{\rm r})\Big|^2, \tag{51}$$

where we have defined

$$W_{\rm A}(\boldsymbol{y}_{\rm s}; \boldsymbol{y}_{\rm r}) = \frac{1}{N}\sum_{n=1}^{N} \exp\Big[2i\frac{\omega_{\rm c}\boldsymbol{x}_n\cdot(\boldsymbol{y}_{\rm s}-\boldsymbol{y}_{\rm r})}{c_0 L} + i\phi^\varepsilon(\boldsymbol{x}_n)\Big]. \tag{52}$$

Compared to the unperturbed (homogeneous and non-dispersive) case, we can easily identify the differences:
- there is a shift in the function $W_{\rm R}$ due to the homogeneous Langmuir frequency. It will be responsible for a shift in the range resolution that is deterministic.
- there are random phases in the terms of the series that determines the function $W_{\rm A}$. They will be responsible for a loss of azimuthal resolution and stability.

The random phase $\phi^\varepsilon(\boldsymbol{x}_n)$ has particular features. Assume that the random processes ν and μ are independent for simplicity. As $\varepsilon \to 0$ the random phase vector indexed by antenna locations, $(\phi^\varepsilon(\boldsymbol{x}_n))_{\boldsymbol{x}_n}$, converges to a stationary Gaussian random process $(\phi(\boldsymbol{x}_n))_{\boldsymbol{x}_n}$ with mean zero and covariance function

$$\mathbb{E}[\phi(\boldsymbol{x}_n)\phi(\boldsymbol{x}_{n'})] = \frac{\omega_{\rm c}^2 L}{c_0^2} C_\mu(\boldsymbol{x}_n - \boldsymbol{x}_{n'}) + \frac{\omega_0^4 L}{\omega_{\rm c}^2 c_0^2} C_\nu(\boldsymbol{x}_n - \boldsymbol{x}_{n'}), \tag{53}$$

where

$$C_\mu(\boldsymbol{x}) = \int_0^1 ds \int_{-\infty}^{\infty} dz \mathbb{E}[\mu(\boldsymbol{0},0)\mu(s\boldsymbol{x},z)], \qquad C_\nu(\boldsymbol{x}) = \int_0^1 ds \int_{-\infty}^{\infty} dz \mathbb{E}[\nu(\boldsymbol{0},0)\nu(s\boldsymbol{x},z)].$$

If we assume that the covariance functions of the stationary random processes ν and μ have the Gaussian forms

$$\mathbb{E}[\mu(\boldsymbol{0},0)\mu(\boldsymbol{x},z)] = \sigma_\mu^2 \exp\Big(-\frac{|\boldsymbol{x}|^2+z^2}{\ell_\mu^2}\Big), \tag{54}$$

$$\mathbb{E}[\nu(\boldsymbol{0},0)\nu(\boldsymbol{x},z)] = \sigma_\nu^2 \exp\Big(-\frac{|\boldsymbol{x}|^2+z^2}{\ell_\nu^2}\Big), \tag{55}$$

then we get

$$\mathbb{E}[\phi(\boldsymbol{x}_n)\phi(\boldsymbol{x}_{n'})] = \frac{\sqrt{\pi}\omega_{\rm c}^2 L}{c_0^2}\sigma_\mu^2\ell_\mu\mathcal{C}\Big(\frac{|\boldsymbol{x}_n-\boldsymbol{x}_{n'}|}{\ell_\mu}\Big) + \frac{\sqrt{\pi}\omega_0^4 L}{\omega_{\rm c}^2 c_0^2}\sigma_\nu^2\ell_\nu\mathcal{C}\Big(\frac{|\boldsymbol{x}_n-\boldsymbol{x}_{n'}|}{\ell_\nu}\Big), \tag{56}$$

with

$$\mathcal{C}(x) = \frac{1}{x}\int_0^x \exp(-s^2)ds = \frac{\sqrt{\pi}}{2x}\mathrm{erf}(x). \tag{57}$$

We can observe that the covariance function of the random phase $\phi(\boldsymbol{x}_n)$ decays very slowly, as the inverse of the distance between the points. This algebraic decay actually holds true for a very large class of covariance functions for μ and ν. For instance, any separable covariance function of the form $\mathbb{E}[\mu(\mathbf{0},0)\mu(\boldsymbol{x},z)] = c_{\mu,1}(\boldsymbol{x})c_{\mu,2}(z)$ with integrable functions $c_{\mu,1}$ and $c_{\mu,2}$ gives rise to the $1/x$-decay for the phase covariance function. In order to simplify the forthcoming analysis, but without loss of generality, we will assume that the covariance functions of the random processes ν and μ have the form (54-55) with $\ell_\mu = \ell_\nu = \ell$ so that the phase covariance function takes the simple form

$$\mathbb{E}[\phi(\boldsymbol{x}_n)\phi(\boldsymbol{x}_{n'})] = \sigma^2\mathcal{C}\Big(\frac{|\boldsymbol{x}_n-\boldsymbol{x}_{n'}|}{\ell}\Big), \tag{58}$$

with

$$\sigma^2 = \frac{\sqrt{\pi}\omega_{\rm c}^2 L}{c_0^2}\sigma_\mu^2\ell_\mu + \frac{\sqrt{\pi}\omega_0^4 L}{\omega_{\rm c}^2 c_0^2}\sigma_\nu^2\ell_\nu. \tag{59}$$

5.1. Range resolution

The analysis of the range resolution follows from the study of the function $|W_{\rm R}(z_{\rm s};z_{\rm r})|^2$ given by (49). It can be seen that the range resolution is not affected by the random fluctuations of the medium and it is still given by the reciprocal of the bandwidth as in the unperturbed non-dispersive case. The only noticeable effect is a shift by the constant $L\omega_0^2/(2\omega_{\rm c}^2)$.

5.2. Azimuthal resolution

The analysis of the azimuthal resolution shows more important differences with respect to the unperturbed case. Let us denote the reflector position $\boldsymbol{y}_{\rm r}$ by $(y_{\rm r},0)$, the search point $\boldsymbol{y}_{\rm s}$ by $(y_{\rm s},0)$, and assume a dense linear array in between points $\boldsymbol{x}_1$ and $\boldsymbol{x}_N$ being respectively $(\pm D/2,0)$. By (51) the azimuthal ambiguity function is

$$\mathcal{I}_{\rm A}(y_{\rm s}) = \Big|W_{\rm A}(\boldsymbol{y}_{\rm s};\boldsymbol{y}_{\rm r})\Big|^2. \tag{60}$$

In the unperturbed case we have

$$\mathcal{I}_{\rm A}(y_{\rm s}) = \Big|\int_{-1/2}^{1/2}\exp\Big[i\frac{2s(y_{\rm s}-y_{\rm r})D\omega_{\rm c}}{c_0 L}\Big]ds\Big|^2 = \mathrm{sinc}^2\Big(\frac{(y_{\rm s}-y_{\rm r})D\omega_{\rm c}}{c_0 L}\Big), \tag{61}$$

where the function sinc is defined by $\mathrm{sinc}(s) = \sin(s)/s$. In the random case the functional that gives the azimuthal resolution is random and it is of the form

$$\mathcal{I}_{\mathrm{A}}(y_{\mathrm{s}}) = \Big| \int_{-1/2}^{1/2} \exp\Big[i \frac{2s(y_{\mathrm{s}} - y_{\mathrm{r}}) D\omega_{\mathrm{c}}}{c_0 L} + i\phi(Ds\boldsymbol{e}_1) \Big] ds \Big|^2, \tag{62}$$

where $\boldsymbol{e}_1 = (1, 0)$. Using the Gaussianity of the phase ϕ the mean of the functional can be expressed in terms of the phase covariance as

$$\mathbb{E}[\mathcal{I}_{\mathrm{A}}(y_{\mathrm{s}})] = 2 \int_0^1 \cos\Big[\frac{2s(y_{\mathrm{s}} - y_{\mathrm{r}}) D\omega_{\mathrm{c}}}{c_0 L} \Big] \exp\Big[-\sigma^2 + \sigma^2 \mathcal{C}(\frac{sD}{\ell}) \Big] (1-s) ds. \tag{63}$$

In particular the maximum of the mean azimuthal functional, that we call mean peak value, is reached at $y_{\mathrm{s}} = y_{\mathrm{r}}$ and it is given by

$$\mathbb{E}[\mathcal{I}_{\mathrm{A}}(y_{\mathrm{r}})] = 2 \int_0^1 \exp\Big[-\sigma^2 + \sigma^2 \mathcal{C}(\frac{sD}{\ell}) \Big] (1-s) ds. \tag{64}$$

The mean peak value as a function of σ for different values of the ratio D/ℓ is plotted in Figure 2a. If σ is small then the mean peak value can be expanded as follows

$$\mathbb{E}[\mathcal{I}_{\mathrm{A}}(y_{\mathrm{r}})] \overset{\sigma \ll 1}{\simeq} 1 - \sigma^2 \mathcal{P}\Big(\frac{D}{\ell}\Big), \tag{65}$$

where the function $\mathcal{P}$ is given by

$$\mathcal{P}\Big(\frac{D}{\ell}\Big) = 2 \int_0^1 \Big(1 - \mathcal{C}(\frac{sD}{\ell}) \Big) (1-s) ds, \tag{66}$$

it is plotted in Figure 2b, and it can be expanded for small and large ratios D/ℓ as

$$\mathcal{P}\Big(\frac{D}{\ell}\Big) = \begin{cases} \dfrac{1}{18} \dfrac{D^2}{\ell^2}, & \text{if } D \ll \ell, \\ 1 - \sqrt{\pi} \dfrac{\ell}{D} \ln \dfrac{D}{\ell}, & \text{if } D \gg \ell. \end{cases} \tag{67}$$

The Half Width at Half Maximum (HWHM) Y_{A} of the mean functional is defined by

$$\mathbb{E}[\mathcal{I}_{\mathrm{A}}(y_{\mathrm{r}} + Y_{\mathrm{A}})] = \frac{1}{2} \mathbb{E}[\mathcal{I}_{\mathrm{A}}(y_{\mathrm{r}})]. \tag{68}$$

The HWHM as a function of σ for different values of the ratio D/ℓ is plotted in Figure 3a. If σ is small then the HWHM can be expanded as follows

$$Y_{\mathrm{A}} \overset{\sigma \ll 1}{\simeq} Y_{\mathrm{A0}} \Big[1 + \sigma^2 \mathcal{R}\Big(\frac{D}{\ell}\Big) \Big], \tag{69}$$

where Y_{A0} is the unperturbed HWHM (ie the HWHM of (61)) given by

$$Y_{\mathrm{A0}} = \alpha \frac{c_0 L}{\omega_{\mathrm{c}} D} \text{ with } \mathrm{sinc}^2 \alpha = \frac{1}{2} \text{ or } \alpha \simeq 1.39, \tag{70}$$

and the function $\mathcal{R}$ is defined by

$$\mathcal{R}\Big(\frac{D}{\ell}\Big) = \Big(\frac{2}{1 - \sqrt{2}\cos(\alpha)} \Big) \int_0^1 \Big(\cos(2\alpha s) - \frac{1}{2} \Big) \mathcal{C}(\frac{sD}{\ell}) (1-s) ds, \tag{71}$$

it is plotted in Figure 3b, and it can be expanded for small and large ratios D/ℓ as

$$\mathcal{R}\Big(\frac{D}{\ell}\Big) = \begin{cases} c_1 \dfrac{D^2}{\ell^2}, & \text{if } D \ll \ell, \\ c_2\sqrt{\pi}\dfrac{\ell}{D}\ln\dfrac{D}{\ell}, & \text{if } D \gg \ell, \end{cases} \tag{72}$$

where $c_1 = [-5/36 + 5/(12\alpha^2) - \sqrt{2-\alpha^2}/(3\alpha^2)]/(1-\sqrt{2-\alpha^2}) \simeq 0.044$, $c_2 = 1/[2(1-\sqrt{2-\alpha^2})] \simeq 0.669$. Note that the fact that the random perturbation ϕ has long-range correlation induces enhanced perturbations in the HWHM (in the form of a log factor) in the regime $D \gg \ell$.

The SNR of the azimuthal functional is defined as

$$\mathrm{SNR} = \frac{\mathbb{E}[\mathcal{I}_{\mathrm{A}}(y_{\mathrm{r}})]}{\mathrm{Var}(\mathcal{I}_{\mathrm{A}}(y_{\mathrm{r}}))^{1/2}}, \tag{73}$$

where $\mathrm{Var}(\mathcal{I}_{\mathrm{A}}(y_{\mathrm{r}})) = \mathbb{E}[\mathcal{I}_{\mathrm{A}}(y_{\mathrm{r}})^2] - \mathbb{E}[\mathcal{I}_{\mathrm{A}}(y_{\mathrm{r}})]^2$ and

$$\begin{aligned}\mathbb{E}[\mathcal{I}_{\mathrm{A}}(y_{\mathrm{r}})^2] &= 4\int_{-1/2}^{1/2} dx \int_{-1/2+|x|}^{1/2-|x|} dy \int_{-1/2}^{1/2} dx' \int_{-1/2+|x'|}^{1/2-|x'|} dy' \\ &\times \exp\Big[-\sigma^2\Big(2 - \mathcal{C}(2y\frac{D}{\ell}) - \mathcal{C}(2y'\frac{D}{\ell}) - \mathcal{C}((x-x'+y-y')\frac{D}{\ell}) - \mathcal{C}((x-x'-y+y')\frac{D}{\ell}) \\ &\quad + \mathcal{C}((x-x'+y+y')\frac{D}{\ell}) + \mathcal{C}((x-x'-y-y')\frac{D}{\ell})\Big)\Big].\end{aligned}$$

The SNR as a function of σ for different values of the ratio D/ℓ is plotted in Figure 4a. If σ is small the SNR can be expanded as follows

$$\mathrm{SNR} \overset{\sigma \ll 1}{\simeq} \sigma^{-2}\Psi(\frac{D}{\ell}), \tag{74}$$

where the function Ψ is defined by

$$\begin{aligned}\Psi(\frac{D}{\ell}) = \Big\{2\int_{-1/2}^{1/2} dx \int_{-1/2+|x|}^{1/2-|x|} dy \int_{-1/2}^{1/2} dx' \int_{-1/2+|x'|}^{1/2-|x'|} dy' \\ \times \Big[\mathcal{C}((x-x'+y-y')\frac{D}{\ell}) + \mathcal{C}((x-x'-y+y')\frac{D}{\ell}) \\ - \mathcal{C}((x-x'+y+y')\frac{D}{\ell}) - \mathcal{C}((x-x'-y-y')\frac{D}{\ell})\Big]^2\Big\}^{-1/2},\end{aligned} \tag{75}$$

it is plotted in Figure 4b, and it can be expanded for small and large ratios D/ℓ as

$$\Psi(\frac{D}{\ell}) = \begin{cases} 9\sqrt{2}\dfrac{\ell^2}{D^2}, & \text{if } D \ll \ell, \\ \Big(\dfrac{D}{\ell \ln \frac{D}{\ell}}\Big)^{1/2}, & \text{if } D \gg \ell. \end{cases} \tag{76}$$

Note that the mean peak value and HWHM are not affected when $D \ll \ell$, and the SNR is very high. Indeed, when $D \ll \ell$, the random perturbation to the point spread function I_n is an overall phase that does not depend on the antenna location $\boldsymbol{x}_n$ and it vanishes when the ambiguity function is evaluated.

The HWHM and SNR are also weakly affected when $D \gg \ell$ because the sum in the ambiguity function contains many independent components and it self-averages. As a

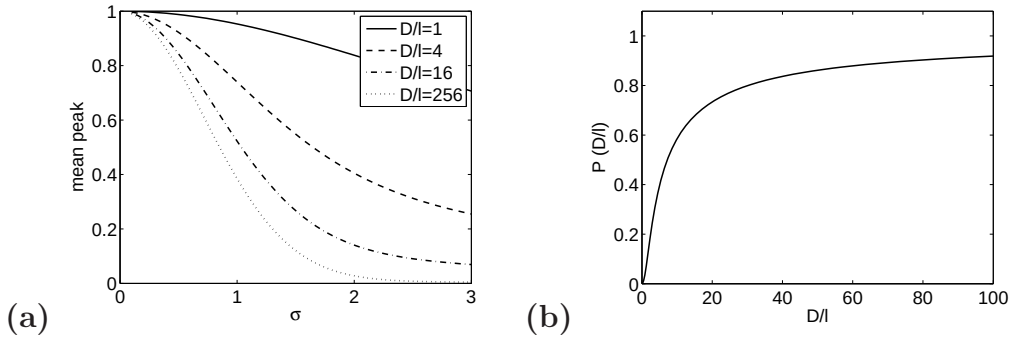

Figure 2. Mean peak value for the azimuthal ambiguity functional (a) and function $\mathcal{P}(D/\ell)$ (b), that gives the correction to the mean peak value for small σ.

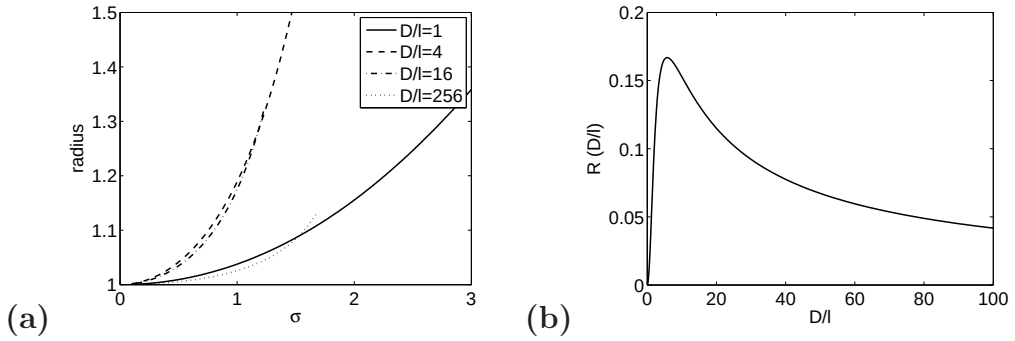

Figure 3. Radius (HWHM) normalized by $Y_{\mathrm{A}0}$ for the azimuthal ambiguity functional (a) and function $\mathcal{R}(D/\ell)$ (b), that gives the correction to the HWHM for small σ. In Figure (a) the radius is plotted as long as the SNR is larger than 2.

result one observes only a decay in the mean peak value but the azimuthal ambiguity functional is statistically stable with a HWHM that is close to the unperturbed value. This self-averaging is, however, not very efficient because the random perturbations have long-range correlations.

Eventually it turns out that the more dramatic effects on the HWHM and SNR due to the random fluctuations of the medium are obtained when $D/\ell \in [5, 20]$ (Figures 3b-4b). This is when the random perturbations of the medium induce the strongest deformations on the azimuthal ambiguity functional.

Note finally that, when σ is large, the picture is very different. In this case the azimuthal imaging functional $\mathcal{I}_{\mathrm{A}}(y_{\mathrm{s}})$ defined by (62) is a speckle pattern, that is, the square modulus of a complex field $\mathcal{E}_{\mathrm{A}}(y_{\mathrm{s}})$ with Gaussian statistics:

$$\mathcal{I}_{\mathrm{A}}(y_{\mathrm{s}}) = |\mathcal{E}_{\mathrm{A}}(y_{\mathrm{s}})|^2.$$

The field $\mathcal{E}_{\mathrm{A}}(y_{\mathrm{s}})$ acquires Gaussian statistics when σ becomes large because the correlation radius of the random process $s \mapsto \exp(i\phi(Ds\boldsymbol{e}_1))$ becomes small (of the order of $\ell/(\sigma D)$ in view of the parameterization of the covariance of the phase ϕ) and the integral in (62) becomes the superposition of many independent components. The

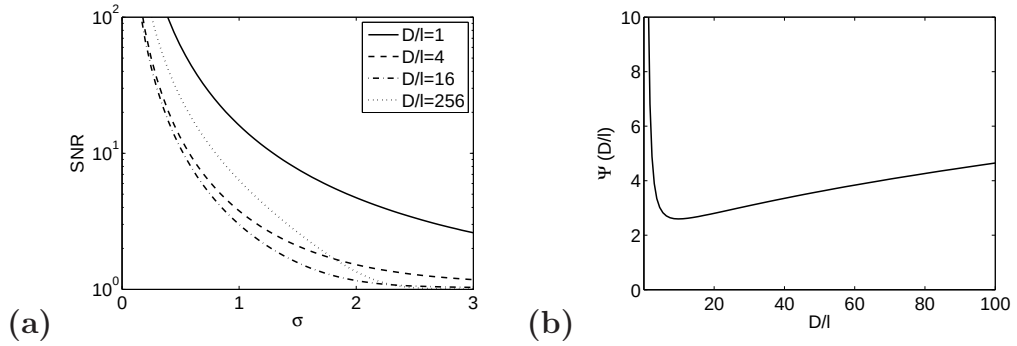

Figure 4. SNR for the azimuthal ambiguity functional (a) and function $\Psi(D/\ell)$ (b), that gives the behavior of the SNR for small σ.

complex field $\mathcal{E}_{\rm A}(y_{\rm s})$ has mean zero and covariance function of the form

$$\mathbb{E}[\mathcal{E}_{\rm A}(y_{\rm s})\overline{\mathcal{E}_{\rm A}(y_{\rm s'})}] = \frac{\sqrt{3\pi}\ell}{\sigma D}\,\mathrm{sinc}\Big(\frac{y_{\rm s'}-y_{\rm s}}{\frac{c_0 L}{D\omega_{\rm c}}}\Big)\,\exp\Big(-\frac{\big(\frac{y_{\rm s}+y_{\rm s'}}{2}-y_{\rm r}\big)^2}{\frac{\sigma^2 c_0^2 L^2}{3\ell^2\omega_{\rm c}^2}}\Big).$$

This means that the field has on the one hand an overall, deterministic, slowly varying envelope with Gaussian shape whose center is $y_{\rm r}$ and whose width is $\frac{\sigma c_0 L}{\sqrt{3}\ell\omega_{\rm c}}$, and on the other hand random, rapid fluctuations with mean zero and correlation radius $\frac{c_0 L}{D\omega_{\rm c}}$. As a result of the complex Gaussian statistics, $\mathcal{I}_{\rm A}(y_{\rm r})$ follows an exponential distribution and the SNR value is one (this can also be seen in Figure 4a). The mean and variance of $\mathcal{I}_{\rm A}(y_{\rm s})$ are

$$\mathbb{E}[\mathcal{I}_{\rm A}(y_{\rm s})] = \frac{\sqrt{3\pi}\ell}{\sigma D}\,\exp\Big(-\frac{(y_{\rm s}-y_{\rm r})^2}{\frac{\sigma^2 c_0^2 L^2}{3\ell^2\omega_{\rm c}^2}}\Big),$$

$$\mathrm{Var}(\mathcal{I}_{\rm A}(y_{\rm s})) = \mathbb{E}[\mathcal{I}_{\rm A}(y_{\rm s})]^2,$$

and its covariance function is

$$\mathrm{Cov}(\mathcal{I}_{\rm A}(y_{\rm s}),\mathcal{I}_{\rm A}(y_{\rm s'})) = |\mathbb{E}[\mathcal{E}_{\rm A}(y_{\rm s})\overline{\mathcal{E}_{\rm A}(y_{\rm s'})}]|^2.$$

Under these conditions SAR imaging gives a speckled image.

6. Conclusions

In the situation with SAR imaging through the earth's ionosphere the image is affected by atmospheric and ionospheric effects. We model these in terms of random fluctuations in the index of refraction and a random Langmuir frequency. We carry out a multiscale analysis motivated by typical scales for atmospheric propagation and identify the scaling regime and distinguished limit in which the effects of the fluctuations can be characterized in terms of a random phase. We use an up/down wave field decomposition to identify the precise form of the correction. In a regime with relatively weak medium fluctuations the effects of the medium fluctuations give a reduction in azimuthal resolution and a reduction in the signal level. These effects can be precisely characterized

in our framework. In the regime of relatively strong medium fluctuations the SAR image becomes a speckle pattern, so that azimuthal resolution is lost, however, the speckle is localized to a band in range with width corresponding to the homogeneous range resolution.

Acknowledgements

This work is partly supported by AFOSR grant # FA9550-11-1-0176, NSF ARRA grant DMS 0908274, and by ERC Advanced Grant Project MULTIMOD-267184.

References

[1] Armand NA 2005 Limitations to the resolution of satellite based synthetic aperture radars due to the conditions of the propagation of radio waves in the ionosphere *Exploration of Earth from Space* **1** 27-38 (in Russian)

[2] Brcic R Parizzi A Eineder M Bamler R and Meyer F 2011 Ionospheric eects in sar interferometry: An analysis and comparison of methods for their estimation *in Proceedings of the 2010 IEEE International Geoscience and Remote Sensing Symposium (IGARSS 2011)*, Vancouver, Canada 1497-1500.

[3] Brown WD and Ghiglia DC 1988 Some methods for reducing propagation-induced phase errors in coherent imaging systems. I. Formalism *J. Opt. Soc. Am. A* **5** 924-941

[4] Carrara WG Goodman RS and Majewski RM 1995 *Spotlight synthetic aperture radar* (Boston: Artech House)

[5] Çetin M and Karl WC 2000 Superresolution and edge-preserving reconstruction of complex-valued synthetic aperture radar images in *Proc. IEEE International Conference on Image Processing* vol 1, Vancouver, Canada 701-704

[6] Chan HL and Yea TS 2002 Noniterative quality phase-gradient autofocus (QPGA) algorithm for spotlight SAR imagery *IEEE Trans. Geo. Rem. Sens.* **36** 1531-1539

[7] Cheney M 2001 A mathematical tutorial on synthetic aperture radar *SIAM Review* **43** 301-312

[8] Curlander JC and McDonough RN 1991 *Synthetic aperture radar* (New York: Wiley)

[9] Cutrona LJ 1990 *Synthetic aperture radar* in Radar Handbook, 2nd ed., Skolnik M, ed. (New York: McGraw Hill)

[10] Derneryd AG Petersson RNO and Ingvarson P 1994 Slotted waveguide antennas for remote sensing satellites *in Proc. of the Progress in Electromagnetic Research Symposium*, Nordwijk, the Netherlands

[11] Eichel PH and Jakowatz Jr CV 1989 Phase-gradient algorithm as an optimal estimator of the phase derivative *Opt. Lett.* **14** 1101-1103

[12] Elachi C 1987 *Spaceborne radar remote sensing* (New York: IEEE Press)

[13] Garnier J and Solna K 2008 Coherent interferometric imaging for synthetic aperture radar in the presence of noise *Inverse Problems* **24** 055001

[14] Garnier J and Solna K 2012 Coupled wideangle wave approximations *SIAM Multiscale Model. Simul.* **10** 217-244

[15] Gilman M Smith E and Tsynkov SV 2013 Reduction of ionospheric distortions for spaceborne SAR with the help of image registration *Inverse Problems: Special issue on Radar Imaging.*

[16] Guyenne TD ed. 1977 *Engineering achievements of ERS-1* European Space Agency SP-11197/III, ESA Publications Division, ESTEC, Noordwijk, the Netherlands

[17] Ishimaru A Kuga Y Liu J Kim Y and Freeman T 1999 Ionospheric effects on synthetic aperture radar at 100 MHz to 2 GHz *Radio Science* **34** 257-268

[18] Koo VC Lim TS and Chuah HT 2005 A comparison of autofocus algorithms for SAR imagery

PIERS Online **1** 16-19 (proceedings of the Progress In Electromagnetics Research Symposium 2005, Hangzhou, China)

[19] Meyer FJ 2011 Performance requirements for ionospheric correction of low-frequency SAR data. *IEEE Transactions on Geoscience and Remote Sensing*, **49(10)** 3694-3702.

[20] Nolan CJ and Cheney M 2002 Synthetic aperture inversion *Inverse Problems* **18** 221-235

[21] Petersson RNO Derneryd AG and Ingvarson P 1994 Microstrip antennas for remote sensing satellites *in Proc. of the Progress in Electromagnetic Research Symposium 1994*, Nordwijk, the Netherlands

[22] Strohbehn JW ed. 1978 *Laser beam propagation in the atmosphere* (Berlin: Springer)

[23] Tsynkov SV 2009 On SAR imaging through the earths ionosphere *SIAM J. Imaging Sciences* **2** 140-182

[24] van Rossum WL Otten MPG and van Bree RJP 2006 Extended PGA for range migration algorithms *IEEE Trans. Aero. Electron. Systems* **42** 478-488

[25] Wahl DE Eichel PH Ghiglia DC and Jakowatz Jr CV 1994 Phase Gradient Autofocus-A robust tool for high resolution SAR phase correction *IEEE Trans. Aero. Electron. Systems* **30** 827-835

[26] Yazici B Cheney M and Yarman CE 2006 Synthetic-aperture inversion in the presence of noise and clutter *Inverse Problems* **22** 1705-1729

[27] Ziomek LJ 1985 *Underwater acoustics: a linear systems theory approach* (Orlando: Academic Press)